Numerical modeling of the electrical breakdown and discharge properties of laser-generated plasma channels

Tz. B. Petrova, H. D. Ladouceur,* and A. P. Baronavski
Molecular Dynamics Section, Chemistry Division, Naval Research Laboratory, 4555 Overlook Avenue, Washington, DC 20375, USA
(Received 21 August 2007; published 21 December 2007)

An extensive nonequilibrium steady-state kinetics model incorporating collisional and radiative processes is developed to study the electrical breakdown and discharge maintenance of laser-induced atmospheric plasma channels formed in externally applied electric fields. The model is based upon a self-consistent numerical solution of the Boltzmann equation for the electron energy distribution function coupled with the electron energy balance equation and the population balance equations for electrons and air species. Using the electron energy distribution function, the ionization and electron attachment rates as a function of the reduced applied electric field at different degrees of ionization are calculated. We find that the ionization rate as a function of applied electric field in a laser-induced plasma channel is orders of magnitude larger than that obtained for a natural atmospheric air discharge. Therefore, the electrical breakdown of these plasma channels may occur at significantly lower applied electric fields. The present model predicts a breakdown electric field of 10 kV/cm, while the experimentally determined breakdown field strength is ~5.7 kV/cm [A. P. Baronavski *et al.*, NRL Memorandum Report No. NRL/MR/6110–02-8642, 2002 (unpublished)], a reduction of about a factor of 5 from the natural Paschen electrical breakdown field of ~30 kV/cm.

DOI: 10.1103/PhysRevE.76.066405 PACS number(s): 52.80.−s, 52.50.Jm, 52.38.Hb, 42.65.Re

I. INTRODUCTION

When an intense femtosecond laser self-focuses in the atmosphere, the air ionizes due to multiphoton or tunneling ionization and one or more low conductivity filamented plasma channels are formed. Specific features of laser beam filamentation, such as long-distance propagation [1–11], white light generation [9], and air breakdown [12–17], have led to many potential technological and scientific applications: high-voltage engineering, ultrabroadband optical generators [18], lightning protection [3,6,17], terahertz radiation generation for spectroscopic and medical applications, pollution control [9,19,20], and remote sensing [21]. To pursue these applications, it is necessary to have a comprehensive quantitative understanding of the physical mechanisms that govern the propagation of intense, ultrashort laser pulses in air and the evolution of the associated plasma channels.

Experiments have shown that femtosecond laser pulses with intensities of tens of Terawatts per square cm produce filaments which can induce and guide electrical discharges between the electrodes of high-voltage sources [6,8,13–16]. The electrons and ions in the plasma channel are created by the laser pulse through the balancing of self-focusing with optical field ionization of air leading to defocusing by the electron density. The self-focusing occurs due to air's intensity dependent nonlinear index of refraction. The specific ionization mechanism depends on the laser field intensity, wavelength, and pulse duration. Guided discharges of several meters in length have been produced by this technique. The initial electron density in the plasma channel is typically $N_e = 10^{16}-10^{17}$ cm^{-3} with a single filament conductivity of ~50 S/m [13]. The plasma channel radius r is approximately 50 μm. The channel dynamics depend on the applied external electric field, electrode separation, and plasma chemistry. Depending on the electrode separation, there are two distinct electrical breakdown cases: (i) long air gaps (>100 cm) where the breakdown and discharge development proceed through a leader mechanism as in lightning on time scales of microseconds [6,19,22]; (ii) short air gaps (≤30 cm) [8,13–15] where the breakdown proceeds without a leader precursor and takes place on a time scale of ~100 ns. Depending on the applied electric field strength in short air gaps, the plasma either decays (subcritical discharge) or breaks down (spark discharge). In a subcritical discharge, the external electric field strength $|\vec{E}|$ is lower then the experimentally observed breakdown field of 5.7 kV/cm [13,15] and the plasma decays via electron-ion recombination and attachment. In the discharge region, the passive current flow obeys Ohm's law $\vec{J}=\sigma\vec{E}$. The current density $\vec{J}$ carried by a single plasma channel of conductivity σ is proportional to the local applied electric field $\vec{E}$ and the total current of multiple channels is additive. If the applied electric field ≥5.7 kV/cm, however, the process of electron multiplication exceeds the electron losses and a bright spark indicative of a breakdown appears with 150–250 ns delay time [13].

The objective of the present investigation is to understand the physics of the breakdown process in a short air gap laser-initiated electrical discharge at atmospheric pressure. In order to accomplish this, we develop a collisional-radiative model based upon the numerical solution of the Boltzmann equation for the electron distribution function $F(\vec{r},\vec{v},t)$, which describes the dependence of the electron number density N_e in $(\vec{r},\vec{v})$ phase space upon an applied electric field $\vec{E}(\vec{r},t)$ and collisional processes,

*Corresponding author; harold.ladouceur@nrl.navy.mil

$$\frac{\partial F(\vec{r},\vec{v},t)}{\partial t} + \vec{v}\cdot\frac{\partial F(\vec{r},\vec{v},t)}{\partial \vec{r}} + \frac{e}{m_e}\vec{E}(\vec{r},t)\cdot\frac{\partial F(\vec{r},\vec{v},t)}{\partial \vec{v}} = \left(\frac{\delta F}{\partial t}\right)_{coll}, \tag{1}$$

where m_e and e are the mass and charge of the electron, respectively. This equation is coupled with balance equations for electrons, ions, and various nitrogen and oxygen species in ground and excited states. We calculate the rates of collisional processes involving electrons over a wide range of discharge conditions, identify significant species and processes associated with the plasma channel dynamics, and determine the conditions for discharge maintenance, plasma decay, or breakdown.

There are several advantages in using a Boltzmann kinetic model to describe the electrical discharge. The laser-initiated air discharges with neutral density N take place at high pressure ($p=1$ atm) and a relatively high degree of ionization ($N_e/N \sim 10^{-4}-10^{-7}$). Unfortunately, published swarm parameters, ionization, and attachment rates are usually obtained at very low degree of ionization ($N_e/N \sim 10^{-15}-10^{-10}$) and consequently cannot be automatically used to model laser-initiated air plasma channel kinetics. In the Boltzmann model, the rate coefficients of all plasma chemical reactions involving electrons are defined as infinite integrals in the velocity space of the product of the collisional cross sections and the electron distribution function. Therefore, the rate coefficients depend on the electron distribution function and consequently they also may change under the action of an applied electric field and collisional events. At moderate degrees of ionization, due to electron-electron collisions, the total ionization rate increases significantly. Moreover, the stepwise participation of the N_2 and O_2 electronically excited states also enhances the total ionization rate by several orders of magnitude compared to the rate at a low degree of ionization. Therefore, it is essential to accurately describe the electron distribution function and its moments. This approach is applicable at any degree of ionization because it uses as input parameters *cross sections* for all reactions involving electrons instead of measured or assumed *collisional rates*. Moreover, the fluid equations for electron number density are directly derived from the Boltzmann equation, being zero- and first-order moments of the electron distribution function.

This paper is organized as follow: Section II describes the kinetic model. In Sec. III, mean electron energy, drift velocity, ionization, and attachment rates obtained from this model are compared with published data at low degrees of ionization. This provides a validation for the model. In addition, the same discharge parameters are calculated as functions of both the reduced electric field E/N and ionization degree N_e/N. The main results from the model, regarding plasma maintenance and breakdown, are further discussed and summarized in Sec. V.

II. KINETIC MODEL

The mathematical model is a reduced version of the complete Boltzmann equation (1) and its moments. To solve this equation an expansion for the distribution function in spherical harmonics is used [23]. The following assumptions are made: (1) the electron distribution function is time-independent due to fast collisional relaxation; (2) the applied electric field in a short air gap is homogeneous; and (3) the electron distribution function is spatially independent. Thus, the electron distribution function depends explicitly upon the electron kinetic energy $u=\frac{1}{2}mv^2$, where v is the absolute value of the electron velocity. Electron-electron collisions are treated as Fokker-Planck terms. The collisional processes between electrons and the air species (both elastic and inelastic) are included via collisional integrals. The ionization events are treated as processes in which the new electron and the incident electron equally share the remainder of electron kinetic energy [24]. The air kinetics model includes a wide variety of physical and chemical processes such as direct excitation and deexcitation, quenching by electrons and heavy particles, ionization, dissociation, attachment, detachment, recombination, charge exchange, diffusion, and radiation. Under these assumptions, an integrodifferential equation for the isotropic component of the electron energy distribution function (EEDF) $f^0(u)$ is obtained,

$$-\frac{d}{du}\left\{\left[\underbrace{\frac{ue^2}{3Q^{\mathrm{tot}}(u)}\left(\frac{E}{N}\right)^2}_{\text{electric field}} + \underbrace{2\Gamma^{ee}\left(\frac{N_e}{N}\right)\left(\int_0^u u'^{3/2}f^0(u')du' + u^{3/2}\int_u^\infty f^0(u')du'\right)}_{\text{electron-electron collisions}}\right]\frac{df^0(u)}{du}\right.$$

$$\left. + \left[\underbrace{u^2\sum_{i=1}^{k}\frac{2m_e}{M_i}\left(\frac{N_i}{N}\right)Q_i^{\mathrm{em}}(u)}_{\text{elastic collisions}} + \underbrace{3\Gamma^{ee}\left(\frac{N_e}{N}\right)\int_0^u u'^{1/2}f^0(u')du'}_{\text{electron-electron collisions}}\right]f^0(u)\right\}$$

$$+\left\{\underbrace{u\sum_{i=0}^{l}\sum_{j=0}^{l}\left(\frac{N_i^*}{N}\right)Q_{ij}^{\mathrm{exc}}(u)}_{\text{excitation}} + \underbrace{u\sum_{i=1}^{l}\sum_{j=0}^{l}\left(\frac{N_i^*}{N}\right)Q_{ij}^{\mathrm{deexc}}(u)}_{\text{deexcitation}} + \underbrace{u\sum_{i=0}^{l-1}\left(\frac{N_i^*}{N}\right)Q_{il}^{\mathrm{ion}}(u)}_{\text{ionization}} + \underbrace{u\sum_{i=\mathrm{O},\mathrm{O}_2,\mathrm{O}_3}\left(\frac{N_i}{N}\right)Q_i^{\mathrm{att}}(u)}_{\text{attachment}}\right\}$$

$$+u\underbrace{\sum_{i=O^-,O_2^-,O_3^-}\left(\frac{N_i}{N}\right)Q_i^{\mathrm{det}}(u)}_{\text{detachment}}+\underbrace{\frac{u^{1/2}}{N}\sqrt{\frac{m_e}{2}}\nu^{\mathrm{dif}}}_{\text{diffusion}}+\underbrace{\frac{u^{1/2}}{N}\sqrt{\frac{m_e}{2}}\sum\nu_i^{\mathrm{rec}}}_{\text{recombination}}\Bigg\}f^0(u)$$

$$=\underbrace{\sum_{i=0}^{l}\sum_{j=0}^{l}(u+U_{ij}^{\mathrm{exc}})\left(\frac{N_i^*}{N}\right)Q_{ij}^{\mathrm{exc}}(u+U_{ij}^{\mathrm{exc}})f^0(u+U_{ij}^{\mathrm{exc}})}_{\text{excitation}}+\underbrace{\sum_{i=1}^{l}\sum_{j=0}^{l}(u-U_{ij}^{\mathrm{exc}})\left(\frac{N_i^*}{N}\right)Q_{ij}^{\mathrm{deexc}}(u-U_{ij}^{\mathrm{exc}})f^0(u-U_{ij}^{\mathrm{exc}})}_{\text{deexcitation}}$$

$$+\underbrace{4\sum_{i=0}^{l-1}(2u+U_{il}^{\mathrm{ion}})\left(\frac{N_i^*}{N}\right)Q_{il}^{\mathrm{ion}}(2u+U_{il}^{\mathrm{ion}})f^0(2u+U_{il}^{\mathrm{ion}})}_{\text{ionization}}. \tag{2}$$

Here $\Gamma^{ee}=\frac{e^2}{24\pi\varepsilon_0}\ln(\Lambda^{ee})$, where $\ln(\Lambda^{ee})$ is the Coulomb logarithm $\Lambda^{ee}=\frac{12\pi}{e^3}\frac{\left(\frac{2}{3}\langle u\rangle\varepsilon_0\right)^{3/2}}{\sqrt{N_e}}$ and ε_0 is the permittivity of free space. M_i, N_i and $Q_{ij}^{process}(u)$ are the mass, number density, and cross sections for the ith species with a superscript being the corresponding process and the subscript denoting the initial state i and final state j; N_i^* is the number density of the excited molecules in energy level i, and U_{ij}^{exc} and U_{il}^{ion} are the excitation (exc) and ionization (ion) threshold of the corresponding process; Q^{tot} is the total transport air cross section that accounts for the air composition, $NQ^{tot}(u)=N_{\mathrm{N}_2}Q_{\mathrm{N}_2}^m(u)+N_{\mathrm{O}_2}Q_{\mathrm{O}_2}^m(u)$. It is evident from Eq. (2) that the EEDF depends on a set of parameters E/N, N_e/N, and N_i^*/N, which require a simultaneous solution of the Boltzmann equation (2) and species balance equations.

The EEDF is normalized $\int_0^\infty\sqrt{u}f^0(u)du=1$ and it is used to calculate various macroscopic plasma properties,

$$\text{mean electron energy } \langle u\rangle=\int_0^\infty u^{3/2}f^0(u)du,$$

$$\text{electron mobility } \mu_e=-\frac{2}{3}\frac{1}{m_e}\int_0^\infty\frac{u^{3/2}}{\nu_m(u)}\frac{df^0(u)}{du}du,$$

$$\text{drift velocity } W\equiv\langle\vec{v}\rangle\equiv\mu_eE=-\frac{2}{3}\frac{E}{m_e}\int_0^\infty\frac{u^{3/2}}{\nu_m(u)}\frac{df^0(u)}{du}du,$$

$$\text{plasma conductivity } \sigma_e=-\frac{2}{3}\frac{e^2N_e}{m_e}\int_0^\infty\frac{u^{3/2}}{\nu_m(u)}\frac{df^0(u)}{du}du,$$

and

$$\text{rate coefficients } k_{ij}^{process}=\sqrt{\frac{2e}{m_e}}\int_0^\infty uQ_{ij}^{process}(u)f^0(u)du.$$

The electron energy balance equation is obtained by multiplication of Eq. (2) for EEDF by $u\sqrt{\frac{2e}{m_e}}$ and integrating over u from zero to infinity giving

$$\underbrace{\frac{\sigma_eE^2}{N_e}}_{\text{Joule heating}}=\underbrace{\sum_i E_i^{el}}_{\text{elastic collisions}}+\underbrace{\sum_i\sum_j E_{ij}^{in}}_{\text{inelastic collisions}}+\underbrace{\langle u\rangle\sum_{positive\ ions}\nu^{rec}}_{\text{recombination}}+\underbrace{\langle u\rangle\nu^{dif}}_{\text{diffusion}}, \tag{3}$$

where

$$E_i^{el}=2\frac{m_e}{M_i}N_i\sqrt{\frac{2}{m_e}}\int_0^\infty u^2Q_i^{em}(u)f^0(u)du\equiv\frac{2m_e}{M_i}\langle u\nu_i^{el}\rangle,$$

$$E_{ij}^{in} = U_{ij}^{in} N_i \sqrt{\frac{2}{m_e}} \int_0^\infty u Q_{ij}^{in}(u) f^0(u) du \equiv U_{ij}^{in} \langle \nu_{ij}^{in} \rangle$$

are the elastic E^{el} and inelastic E^{in} electron energy losses with energy threshold U_{ij}^{in}. Analogous equations can be obtained for the species steady-state population balance equations. The electron population balance equation is similarly obtained by multiplication of Eq. (2) by $N_e \sqrt{\frac{2e}{m_e}}$, followed by integration over u from zero to infinity,

$$\underbrace{\sum_s k_s^{ion}\left(\frac{E}{N}, \frac{N_e}{N}\right) N_s N_e}_{\text{ionization}} + \underbrace{\sum_s k_s^{ai} N_s^2}_{\text{associative ionization}} + \underbrace{\sum_{n=\text{negative ions}} k_n^{det}\left(\frac{E}{N}, \frac{N_e}{N}\right) N_n N_e}_{\text{detachment}}$$

$$= \underbrace{\sum_{p=\text{positive ions}} k_p^{rec}\left(\frac{1}{\sqrt{\langle u \rangle}}\right) N_p N_e}_{\text{recombination}} + \underbrace{\sum_{m=\text{O},\text{O}_2,\text{O}_3} k_m^{att}\left(\frac{E}{N}, \frac{N_e}{N}\right) N_m N_e}_{\text{attachment}} + \underbrace{\nu^{dif}(r) N_e}_{\text{diffusion}}. \quad (4)$$

The rate coefficients depend on E/N and N_e/N through the electron energy distribution function $f^0(u)$.

The electron Boltzmann equation is solved for $f^0(u)$ using a conventional numerical technique based upon second-order finite-difference discretization [25,26]. This solution satisfies both the electron population and electron-energy balance equations via self-consistent coupling with the steady-state balance equations for various nitrogen and oxygen species in the ground and electronically excited molecular states. Vibrationally excited states for oxygen and nitrogen are each treated as one lumped level. Atomic and molecular ions are also included (see Table I). The references for all electron cross sections and heavy particle collisional rates are summarized in Table II. In addition, there are more plasmochemical collisional processes between air species that contribute in the species balance equations via reaction rates listed in Table III together with references. More than 300 reactions are included. The radiative processes, responsible for excited states depletion, are treated via the effective radiative lifetimes given in Table IV.

III. RESULTS AND DISCUSSIONS

The model was used to study the electrical discharge of a laser-induced plasma channel by two different approaches.

(i) First approach: Study the discharge dependence on applied electric field at an *a priori* given degree of ionization N_e/N. This provides all plasma characteristics as a function of the reduced applied electric field E/N, used as an input parameter in the code.

(ii) Second approach: The electric field required to maintain the discharge at fixed degrees of ionization N_e/N is determined self-consistently from the electron particle balance equation. This approach allows a seamless transition from the natural breakdown to the plasma channel breakdown.

Common input parameters for these two approaches described above are the ambient initial gas temperature T_g, the plasma channel radius r, cross section data $Q_{ij}^{process}(u)$ for the collisional reactions with electrons, and rates for the air species interactions.

The ionization and attachment rates are the most relevant and important rates in the breakdown process. The total ionization rate, accounting for both direct and step-wise ioniza-

TABLE I. Air plasma species: ionization potential for positive ions, affinity for negative oxygen ions, and excitation threshold for the electronically excited molecular states. The neutral air species included in the model are $N(^4S)$, N_2 $(X\,^1\Sigma_g^+, v=0)$, O $(^3P_2)$, O_2 $(X\,^3\Sigma_g^-, v=0)$, and O_3 $(^1A_1)$.

Air species	Energy (eV)
N_2 $(X\,^1\Sigma_g^+, v=1)$	1.0
N_2 $(A\,^3\Sigma_u^+)$	6.169
N_2 $(B\,^3\Pi_g)$	7.353
N_2 $(W\,^3\Delta_u)$	7.362
N_2 $(B'\,^3\Sigma_u^-)$	8.165
N_2 $(a'\,^1\Sigma_u^-)$	8.399
N_2 $(a\,^1\Pi_g)$	8.549
N_2 $(w\,^1\Delta_u)$	8.890
N_2 $(C\,^3\Pi_u)$	11.032
N_2 $(b\,^1\Pi_u + b'\,^1\Sigma_u^+ + c'\,^1\Sigma_u^+)$	12.763
N^+	14.5341
N_2^+	15.5808
N_4^+	10.3
O_2 $(X\,^3\Sigma_g^-, v=1)$	0.196
O_2 $(a\,^1\Delta_g)$	0.977
O_2 $(b\,^1\Sigma_g^+)$	1.627
O_2 $(c\,^1\Sigma_u^- + A\,^3\Sigma_u^+)$	4.185
O_2 $(B\,^3\Sigma_u^-)$	6.120
O_2 (Rydberg)	9.300
O^+	13.6181
O_2^+	12.072
O^-	−1.461
O_2^-	0.44
O_3^-	2.98

TABLE II. Collisional processes involving electrons. X denotes either nitrogen or oxygen. The * symbol denotes excited states listed in Table I.

Reaction	Nitrogen	Oxygen
Momentum transfer:		
$e+X_2 \rightarrow e+X_2$	Itikawa [34]	Hake and Phelps [36]
	Pitchford and Phelps [35]	
Vibrational excitation:	$n=45$	$n=4$
$e+X_2(v=0) \rightarrow e+X_2(\Sigma_{i=1}^{n} v_i)$	Capitelli *et al.* [37]	Hake and Phelps [36]
Rotational excitation:		
$e+X_2 \rightarrow e+X_2$ (rot exc)	Capitelli *et al.* [37]	Myers [38]
Molecular states excitation:		
$e+X_2 \rightarrow e+X_2^*$	Itikawa [34], Capitelli *et al.* [37]	Capitelli *et al.* [37]
	Shemanski and Broadfood [39]	
Ionization:		
$e+X \rightarrow e+e+X^+$	Brook *et al.* [40]	Brook *et al.* [40]
$e+X_2 \rightarrow e+e+X_2^+$	Itikawa [34]; Capitelli *et al.* [37]	Capitelli *et al.* [37]
$e+X_2^* \rightarrow e+e+X_2^+$	Drawin [41]	Drawin [41]
Attachment:		
$e+O_2 \rightarrow O^-+O$		McDaniel [42]
$e+O_2(a\ ^1\Delta_g) \rightarrow O^-+O$		Burrow [43]
Detachment:		
$e+O^- \rightarrow O$		Jinno *et al.* [44]
$e+O_2^- \rightarrow O_2$		

tion, is calculated as a sum over all ionization processes considered in the Boltzmann equation. The validity of the model was verified at low degrees of ionization ($N_e/N \sim 10^{-15}-10^{-10}$) by comparing published swarm parameters with the model predictions for a dry air discharge at atmospheric pressure. The results are plotted in Fig. 1 as a function of the reduced applied electric field E/N in units of Td (Townsend, 1 Td$=10^{-17}$ V cm^2) and summarized as follows:

(a) Drift velocity W compared with Phelps' model [27] and Dutton's experiments [28] [Fig. 1(a)].

(b) Mean electron energy $\langle u \rangle$ compared with Phelps model [Fig. 1(b)].

(c) Townsend's ionization coefficient α in (cm^{-1}) normalized by the number density, $\frac{\alpha}{N}=\frac{\Sigma_i \nu_i^{\mathrm{ion}}}{WN}$ in (cm^2) [Fig. 1(c)].

(d) Attachment coefficient η in (cm^{-1}) normalized by the number density, $\frac{\eta}{N}=\frac{\Sigma_j \nu_j^{\mathrm{att}}}{WN}$ in (cm^2) [Fig. 1(d)] compared with Phelps model, Gupta's analytical formulas [29], and Lowke's model [30].

In this representation, $\nu_m(u)$ is the total collision frequency of electrons with neutral and charged particles, $\nu_i^{\mathrm{ion}}=k_i^{\mathrm{ion}}N$, and $\nu_j^{\mathrm{att}}=k_j^{\mathrm{att}}N_j$ are the ionization and attachment rates in (s^{-1}), W is the drift velocity in (cm s^{-1}), and N_i or N_j are the species densities of the corresponding collisional partner in (cm^{-3}). As shown in Fig. 1, the code accurately reproduces the swarm parameters and rates available from the literature at a low degree of ionization.

The discharge parameters mentioned above are applicable for studying natural air breakdown initiated at low degrees of ionization $\left(\frac{N_e}{N} \sim 10^{-15}-10^{-10}\right)$. However, as shown in Fig. 2, at high degrees of ionization these parameters are, in general, functions of both E/N and N_e/N. The Maxwellization of the EEDF with an elevated high-energy tail and step-wise ionization results in much larger ionization rate coefficients than the conventional Townsend rate coefficient obtained at lower electron densities. For example, at a reduced electric field of 20 Td, where a one atmosphere air plasma channel breakdown occurs, the total ionization ratio $\frac{\alpha}{N}$ [Fig. 2(c)] calculated numerically by the Boltzmann code is $\frac{\alpha}{N} \sim 10^{-19}$ cm^2 at $\frac{N_e}{N}=4\times10^{-6}$, while at low degree of ionization, at $\frac{N_e}{N}=4\times10^{-10}$, it is $\frac{\alpha}{N} \sim 10^{-27}$ cm^2. The total attachment ratio $\frac{\eta}{N}$ varies from 10^{-18} to 10^{-20} cm^2 and its characteristic minimum, formed by the intersection of the three-body attachment with the two-body attachment, shifts toward lower reduced electric fields as N_e/N increases [Fig. 2(d)]. Also seen in Fig. 2, the drift velocity (a) and the mean energy (b) are both of functions E/N and N_e/N, although the drift velocity exhibits only a weak dependence. The stronger dependence at elevated electron densities is a result of the importance of electron-electron collisions on the EEDF.

The determination of the required electric field to sustain the discharge at fixed degrees of ionization N_e/N is determined by self-consistently solving the Boltzmann equation and the electron particle balance equation. The discharge maintenance concept is based on a balance between electron production and electron loss. In our model, the electron gain from ionization and detachment equals the electron loss through attachment, recombination, and diffusion. The numerical calculations for a preformed plasma channel have been performed under the following discharge conditions:

TABLE III. Rates of plasmochemical reactions involving air species.

Chemical reactions	References
N_2^* in collision with N, N_2, and N_2^*:	Capitelli *et al.* [37]; Guerra and Loureiro [45]; Sá and Loureiro [46]; Piper [47–49]; De Sousa *et al.* [50]
N_2^* in collision with O, O_2, and O_2^*:	Capitelli *et al.* [37]; Guerra and Loureiro [45]; Marinelli *et al.* [51,52]; Iannuzzi *et al.* [53]
O_2^* in collision with O, O_2, O_2^*, and O_3:	Ivanov *et al.* [54]; Gudmundsson *et al.* [55] Capitelli *et al.* [37]; Gordietz *et al.* [56]; Guerra and Loureiro [45]; Feoktistov *et al.* [57]; Kossyi *et al.* [58]
Three-body collisions:	Ivanov *et al.* [54]; Capitelli *et al.* [37]; Guerra and Loureiro [59]; Partridge *et al.* [60]
Neutral dissociation:	Capitelli *et al.* [37]; Guerra and Loureiro [59]
Associative ionization:	Guerra and Loureiro [45]; Gordietz *et al.* [61]
Reactions involving positive ions (charge exchange, recombination, and dissociation):	Capitelli *et al.* [37]; Kossyi *et al.* [58]; Guthrie *et al.* [62]; Zinn *et al.* [63]; McDaniel *et al.* [64]; Niels [65]
Dissociative recombination:	Kossyi *et al.* [58]
Attachment:	Hayashi and Kadota [66]; Feoktistov *et al.* [57]; Kossyi *et al.* [58]; Chanin *et al.* [67]; Chanin *et al.* [68]
Collisional detachment:	Ivanov *et al.* [54]; Gudmundsson *et al.* [55]; Capitelli *et al.* [37]; Feoktistov *et al.* [57]; Upschulte *et al.* [69]; Steinfeld *et al.* [70]
Reactions involving negative ions (charge exchange, recombination, and dissociation):	Ivanov *et al.* [54]; Capitelli *et al.* [37]; Feoktistov *et al.* [57]; Kossyi *et al.* [58]; Ichikawa *et al.* [71]; Fehsenfeld *et al.* [72]
Mutual neutralization (ion-ion recombination):	Capitelli *et al.* [37]; Feoktistov *et al.* [57]; Kossyi *et al.* [58]; Niels [65]
Three-body ion-ion recombination:	Ivanov *et al.* [54]; Capitelli *et al.* [37]; Kossyi *et al.* [58]

gas temperature $T_g=300$ K, gas pressure $p=1$ atm, and plasma channel radius $r=50$ μm ($pr=3.8$ Torr cm). The EEDF f^0 is shown in Fig. 3 as a function of the electron energy u and ionization degree N_e/N. The resulting distribution arises from the interplay between energy gain from the electric field and energy loss through various collisional processes. Inelastic collisions of electrons with nitrogen molecules control the shape of the EEDF, while oxygen acts as both a source and sink of electrons through ionization, attachment, and detachment. At low degrees of ionization an enhanced tail of the EEDF is possible at the expense of increasing the electric field strength to $E/N=120$ Td (cf. Fig. 6 for details on maintaining electric field E_{sc} as a function of degree of ionization N_e/N). At high degrees of ionization, even at moderate field strength ($E/N\simeq 25$ Td), the tail of the EEDF is enhanced because of the increasing importance of the electron-electron collisions.

The rates participating in the electron balance equation vs degree of ionization are plotted in Fig. 4. The electrons, created due to ionization and detachment, are lost by attachment, recombination, and radial diffusion. The total ionization frequency includes direct ionization from O, N, O_2, and N_2, stepwise ionization from all electronically excited nitrogen and oxygen molecular states under consideration, and associative ionization. Details on the attachment-detachment dependence are given in Fig. 4(a), while in Fig. 4(b), the net attachment frequency is plotted as the difference between attachment and detachment frequencies. It is seen from Fig. 4 that the ionization frequency reaches a minimum of $\nu_{\min}^{\text{ion}}=6\times 10^6$ s^{-1} for $N_e/N=2\times 10^{-8}$, that is, the field can be sustained with minimal production of electrons. At higher degrees of ionization ($>5\times 10^{-5}$), the electron loss is primarily due to dissociative recombination.

TABLE IV. Radiative processes and lifetimes [37].

Transition $n \rightarrow m$	$A_{v=0}^{nm}$ (s^{-1})	Wavelength for $v \rightarrow v'$
Nitrogen		
$N_2\ (A\ ^3\Sigma_u^+) \rightarrow N_2\ (X\ ^1\Sigma_g^+) + \hbar\nu$	0.5	293 nm, $0 \rightarrow 7$
$N_2\ (B\ ^3\Pi_g) \rightarrow N_2\ (A\ ^3\Sigma_u^+) + \hbar\nu$	1.34×10^5	1045 nm, $0 \rightarrow 0$
$N_2\ (W\ ^3\Delta_u) \rightarrow N_2\ (X\ ^1\Sigma_g^+) + \hbar\nu$	0.154	208 nm, $0 \rightarrow 5$
$N_2\ (B'\ ^3\Sigma_u^-) \rightarrow N_2\ (B\ ^3\Pi_g) + \hbar\nu$	3.4×10^4	1524 nm, $0 \rightarrow 0$
$N_2\ (C\ ^3\Pi_u) \rightarrow N_2\ (B\ ^3\Pi_g) + \hbar\nu$	2.45×10^7	336.5 nm, $0 \rightarrow 0$
$N_2\ (a'\ ^1\Sigma_u^-) \rightarrow N_2\ (X\ ^1\Sigma_g^+) + \hbar\nu$	1.0×10^2	177.1 nm, $0 \rightarrow 5$
$N_2\ (a\ ^1\Pi_g) \rightarrow N_2\ (X\ ^1\Sigma_g^+) + \hbar\nu$	8.55×10^3	155.2 nm, $0 \rightarrow 2$
$N_2\ (a\ ^1\Pi_g) \rightarrow N_2\ (a'\ ^1\Sigma_u^-) + \hbar\nu$	1.3×10^2	8252 nm, $0 \rightarrow 3$
$N_2\ (w\ ^1\Delta_u) \rightarrow N_2\ (a\ ^1\Pi_g) + \hbar\nu$	1.51×10^3	3578 nm, $0 \rightarrow 0$
$N_2\ (b\ ^1\Pi_u) \rightarrow N_2\ (X\ ^1\Sigma_g^+) + \hbar\nu$	7.7×10^8	111.6 nm, $0 \rightarrow 5$
$N_2\ (b\ ^1\Pi_u) \rightarrow N_2\ (a\ ^1\Pi_g) + \hbar\nu$	1.59×10^8	313.3 nm, $0 \rightarrow 0$
$N_2\ (b'\ ^1\Sigma_u^+) \rightarrow N_2\ (X\ ^1\Sigma_g^+) + \hbar\nu$	4.8×10^8	135.4 nm, $0 \rightarrow 14$
$N_2\ (b'\ ^1\Sigma_u^+) \rightarrow N_2\ (a\ ^1\Pi_g) + \hbar\nu$	5.56×10^5	353.1 nm, $0 \rightarrow 4$
Oxygen		
$O_2\ (a\ ^1\Delta_g) \rightarrow O_2\ (X\ ^3\Sigma_g^-) + \hbar\nu$	2.6×10^{-4}	1.27 μm
$O_2\ (b\ ^1\Sigma_g^+) \rightarrow O_2\ (a\ ^1\Delta_g) + \hbar\nu$	1.5×10^{-3}	1.9 μm
$O_2\ (b\ ^1\Sigma_g^+) \rightarrow O_2\ (X\ ^3\Sigma_g^-) + \hbar\nu$	1.5×10^{-3}	762 nm
$O_2\ (c\ ^1\Sigma_u^- + A'\ ^3\Delta_u + A\ ^3\Sigma_u^+) \rightarrow O_2\ (a\ ^1\Delta_g) + \hbar\nu$	11	243–306 nm
$O_2\ (B\ ^3\Sigma_u^-) \rightarrow O_2\ (X\ ^3\Sigma_g^-) + \hbar\nu$	2×10^6	200 nm

The power gain per electron from the electric field due to Joule heating and the partial contribution to the power loss of different elastic and inelastic processes (electron power balance) vs degree of ionization N_e/N is presented in Fig. 5. Plotted are the normalized net excitation and vibrational excitation rates (excitation minus deexcitation), ionization, attachment, rotational excitation, and ambipolar diffusion. The energy loss is dominated by two competitive processes, namely vibrational excitation and electronic excitation of O_2 and N_2. The energy transfer back to the electrons has been taken into account via deexcitation and detachment processes. For high degrees of ionization, part of the energy utilized in vibrational excitation is returned back to the electrons via deexcitation from vibrationally excited molecules. The fraction of returned energy can be nearly 100% at high degrees of ionization, when the vibrational temperature approaches the electron temperature, resulting in lower power loss and consequently, lower maintaining field.

The self-consistent electric field E_{sc} required to maintain a steady-state electrical discharge vs degree of ionization is plotted in Fig. 6. As mentioned above, we define the self-consistent electric field strength as the field for which the electron production via ionization and detachment is balanced by the electron loss via recombination and attachment. The left side of the self-consistent field curve, degree of ionization 10^{-15}, corresponds to the natural breakdown field in air, ~ 30 kV cm^{-1}. Breakdown is initiated at any point above 30 kV cm^{-1}; consequently, an electric field equal or larger than $E_{crit}=30$ kV cm^{-1} is required. During a natural breakdown the electron density (the ionization degree) increases exponentially and reaches the maximum value determined by the net system impedance, e.g., the electron density must shift from the corresponding lower degree of ionization (A) toward higher degrees of ionization (B) (Fig. 6).

The right side of the self-consistent electric field curve (Fig. 6) corresponds to a plasma channel breakdown. In our experiments the initial degree of ionization produced by the laser is on the order of 10^{-3} [8], corresponding to an initial electron density $\sim 10^{16}$ cm^{-3} [7,8,12]. Experimentally, the electrical discharge does not occur instantly even if the applied electric field is sufficient for an electron avalanche to develop. The time lag in a dc electric field is found experimentally to be 150–250 ns [13]. The ionization rate at the minimum maintaining field is $\sim 10^7$ s^{-1}. The model predicts that the breakdown time is ~ 200 ns (a few times the inverse ionization rate), close to what is observed experimentally. This initial electron density decays to 10^{10}–10^{12} via recombination and attachment before the breakdown initiates. In Fig. 6 this corresponds to a shift of the maintaining electric field from right to left (E-D-C). The self-consistent electric field is about 10 kV/cm at degrees of ionization 10^{-6}–10^{-7} and this may be considered as optimum breakdown electric field, about one third of the natural breakdown field. It may be noted that a similar maintaining field dependence was predicted by Lowke, who plots the reduced electric field E/N versus current density J [30]. Lowke's reduced electric field reaches minimum at much lower electron densities and the minimum reduced electric field itself is lower than ours. However, in his analysis, Lowke adjusts the value of the ionization rate so that the curve $E/N(J)$ goes through a minimum at 20 Td, a value known *a priori* from other experiments [31]. Presumably these assumptions are dictated by the limited air chemistry used in his model.

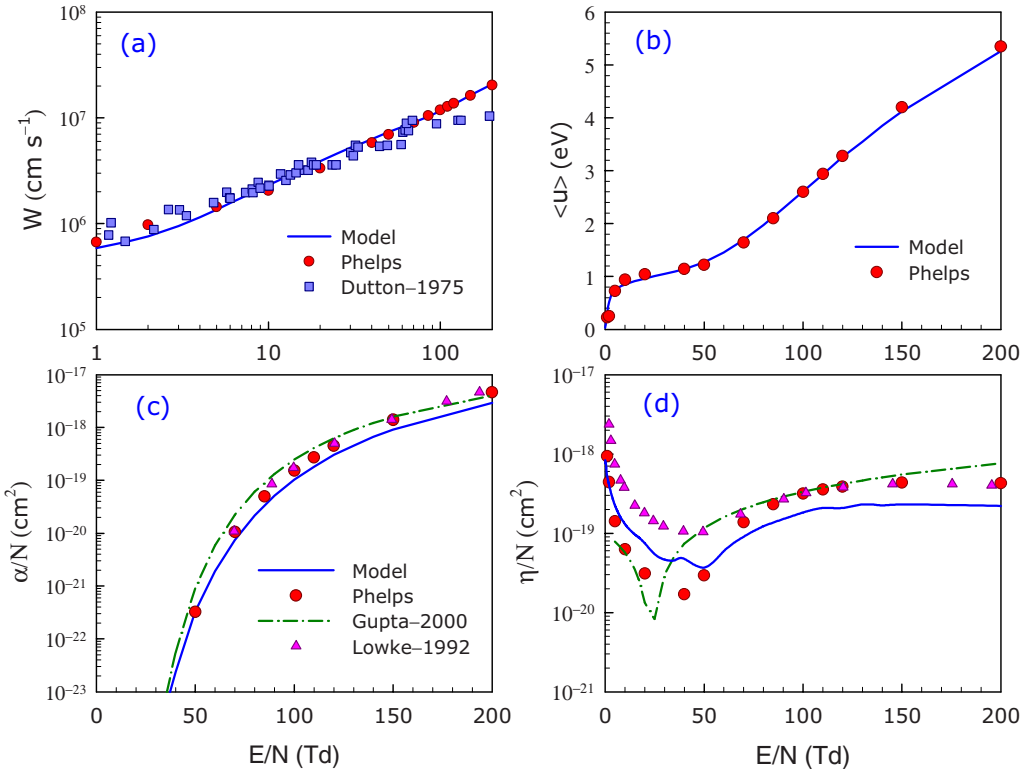

FIG. 1. (Color online) Discharge parameters in 1 atm air as a function of the reduced electric field E/N and vanishing degree of ionization N_e/N (first approach): drift velocity W (a), mean electron energy $\langle u \rangle$ (b), Townsend's ionization coefficient α in (cm^{-1}) normalized by the number density: the ratio α/N (c), and total attachment versus number density: the ratio η/N (d).

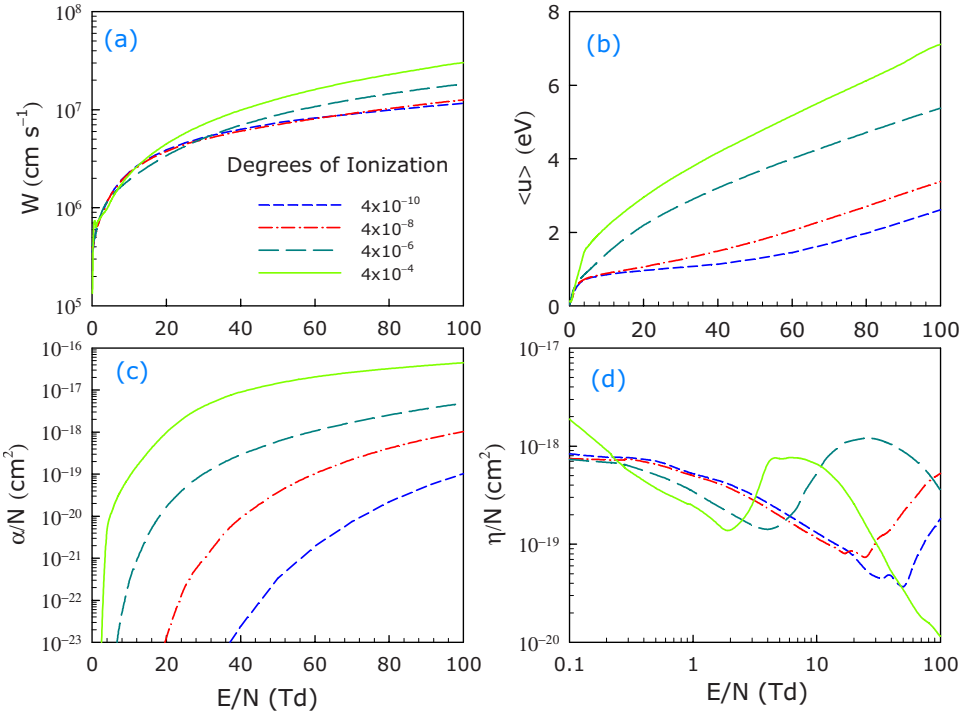

FIG. 2. (Color online) Discharge parameters in 1 atm air as a function of both the reduced electric field E/N for various degrees of ionization N_e/N: drift velocity W (a), mean electron energy $\langle u \rangle$ (b), Townsend's ionization coefficient α in (cm^{-1}) normalized by the number density: the ratio α/N (c), and total attachment versus number density: the ratio η/N (d).

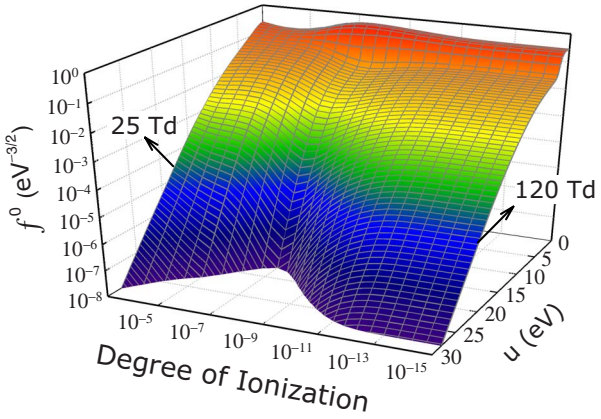

FIG. 3. (Color online) Electron energy distribution function $f^0(u)$ at various degrees of ionization N_e/N (second approach). Discharge conditions: gas pressure $p=1$ atm, gas temperature $T_g=300$ K, and plasma channel radius $r_0=50$ μm.

The experimentally observed breakdown electric field for the laser-induced plasma channel measured is 5.7 kV/cm (a reduced breakdown electric field of 23 Td) [13,15]. The minimum maintaining field of 10 kV/cm calculated by the model requires an additional mechanism to explain this discrepancy. The gas heating mechanism has already been successfully employed in various breakdown models [12,32,33]. Tzortzakis *et al.* [32] showed that the gas heats during breakdown. They measured a gas heating rate of approximately 1.2 K/ns in air at one atmosphere pressure. In a similar study, Popov [22] estimates a heating rate of 3 K/ns for a leader channel. Even for the more conservative heating rate [32], in ~200 ns the gas temperature would reach 500–600 K, reducing the normalized breakdown electric field E/N twice.

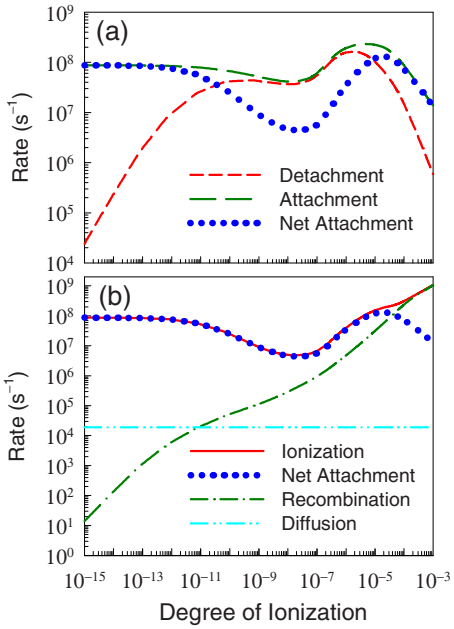

FIG. 4. (Color online) Attachment, detachment, and net attachment rates (a) and electron creation and loss rates (b) vs degree of ionization N_e/N. The discharge conditions are the same as in Fig. 3.

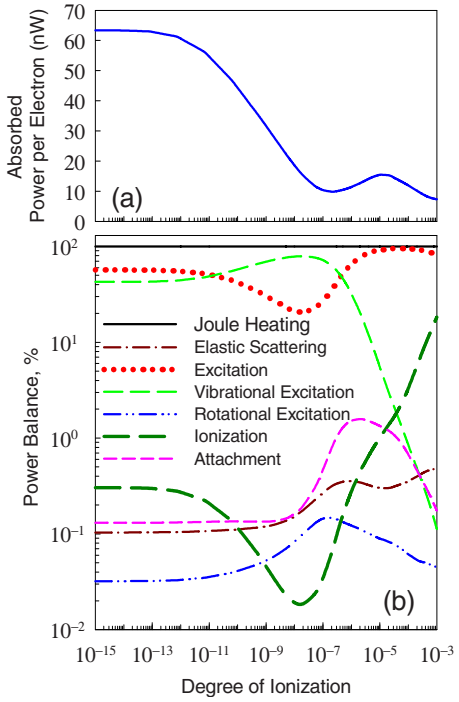

FIG. 5. (Color online) Power loss per electron (a) and power balance distribution (b) vs degree of ionization N_e/N. The discharge conditions are the same as in Fig. 3.

Our model was used to predict the gas temperature ~200 ns after the laser pulse. A simplified gas temperature balance equation accounting for heating arising only due to vibrational kinetics reads $\frac{d}{dt}\left(\frac{3}{2}NT_g(t)\right)=\xi k^{\mathrm{vib}}N_e(t)N\Delta E^{\mathrm{vib}}$, where k^{vib} and ΔE^{vib} are the rate coefficient and effective energy threshold for electron impact vibrational excitation, respectively. The parameter ξ is the fraction of the power transferred to the gas. The temporal evolution of the electron density was taken from experiment, where a suitable fit was

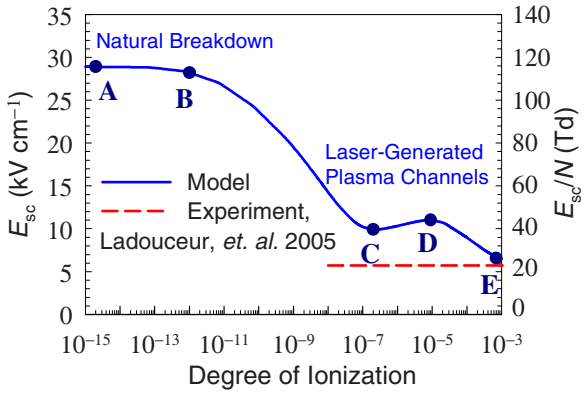

FIG. 6. (Color online) Discharge maintaining electric field E_{sc} vs degree of ionization N_e/N. The discharge conditions are the same as in Fig. 3. *A*—natural air breakdown initiation; *AB*—air discharge. (*B* may shift right. The shift is determined by the system impedance.) *C*—laser-induced plasma channel breakdown; *EDC*—in this region, for laser-induced plasma channels, the initial electron density drops. (*E* may shift. The shift depends on the laser intensity and self-focusing properties.)

made to N_e through the equation $N_e(t)=1.25\times10^{16}\exp(-6.84\times10^6 t)/(1+4.65\times10^8 t)$ [8]. An integration of the gas temperature equation yields $T_g(t)=T_0+\xi k^{\mathrm{vib}}\Delta E^{\mathrm{vib}}\int_0^t N_e(t')dt'$. Assuming $\xi\approx0.05$ [33], with the integral of the electron density being 1×10^8 cm^{-3} s, $k^{\mathrm{vib}}\approx8\times10^{-9}$ cm^{-3}, and $\Delta E^{\mathrm{vib}}\approx1$ eV (for N_2), we find that after $t\approx200$ ns the gas temperature is $T_g\approx600$ K (a heating rate of ~1.5 K/ns [22]). Gas heating of this magnitude will increase the minimum of the normalized applied field from $E/N\approx23$ Td at $T_g=300$ K to $E/N\approx46$ Td after ~200 ns. According to the model predictions (Fig. 6), at a normalized electric field $E/N\approx46$ Td breakdown is readily possible. Thus, the model may be used to explain why the discharge "waits" ~200 ns for the breakdown to occur.

From the dependence of E/N vs N_e/N (Fig. 6) it is clear that breakdown is possible for $E/N>40$ Td. For lower normalized electric fields the possibility for breakdown is determined by two competitive processes: gas heating, leading to an increase with time of the applied reduced electric field E/N, and decay of the electron density, leading to plasma extinction. Apparently, the definitive answer whether breakdown occurs or not for $E/N<40$ Td is only possible if the model is time-dependent and accounts for a gas heating.

IV. SUMMARY

In conclusion, a collisional-radiative air chemistry code based upon the numerical solution of the steady-state electron Boltzmann equation is developed to model laser-induced plasma channel discharges at atmospheric pressure. These air plasma channels operate at elevated degrees of ionization $\left(\frac{N_e}{N}\sim10^{-4}-10^{-7}\right)$ and the EEFD is a function of two parameters: E/N and N_e/N. Consequently, all plasma properties become functions of these two parameters. A high total ionization rate, exceeding the net attachment plus recombination rates was obtained at substantially lower electric field strength (40 Td) due to the Maxwellization of the EEDF as a result of electron-electron collisions. The total ionization rate is increased orders of magnitude over that obtained for a one-atmosphere natural air discharge.

The present model provides a bridge between the natural and plasma channel breakdown. The combination of Boltzmann analysis and gas heating can explain why plasma channel breakdown occurs at an applied electric field five times lower than the critical field for dielectric breakdown in air at one atmosphere (28–30 kV/cm). The model suggests that the observed time lag for the plasma channel breakdown is due to two factors: electron avalanche development (an ionization time of ~200 ns) and increase in the ratio E/N due to gas heating. Future work will include detailed vibrational kinetics, gas heating, and ultimately, time dependent Boltzmann analysis.

ACKNOWLEDGMENT

This work is supported by the Office of Naval Research.

[1] A. Braun, G. Korn, X. Liu, D. Du, J. Squier, and G. Mourou, Opt. Lett. **20**, 73 (1995).
[2] X. M. Zhao, J.-C. Diels, C. Y. Wang, and J. M. Elizondo, IEEE J. Quantum Electron. **31**, 599 (1995).
[3] M. Miki and A. Wada, J. Appl. Phys. **80**, 3208 (1996).
[4] B. La Fontaine, F. Vidal, Z. Jiang, C. Y. Chien, D. Comtois, A. Desparois, T. W. Johnston, J. C. Kieffer, H. Pepin, and H. P. Mercure, Phys. Plasmas **6**, 1615 (1999).
[5] H. Schillinger and R. Sauerbrey, Appl. Phys. B: Lasers Opt. **68**, 753 (1999).
[6] F. Vidal, D. Comtois, C. Y. Chien, A. Desparois, B. La Fontaine, T. W. Johnston, J. C. Kieffer, H. P. Mercure, H. Pepin, and F. A. Rizk, IEEE Trans. Plasma Sci. **28**, 418 (2000).
[7] S. Tzortzakis, B. Prade, M. Franco, and A. Mysyrowicz, Opt. Commun. **181**, 123 (2000).
[8] H. D. Ladouceur, A. P. Baronavski, D. Lohrmann, P. W. Grounds, and P. G. Girardi, Opt. Commun. **189**, 107 (2001).
[9] J. Kasparian, M. Rodriguez, G. Mejean, J. Yu, E. Salmon, H. Wille, R. Bourayou, S. Frey, Y. B. Andre, A. Mysyrowicz, R. Sauerbrey, J. P. Wolf, and L. Woste, Science **301**, 61 (2003).
[10] S. L. Chin, S. A. Hosseini, W. Liu, Q. Luo, F. Théberge, N. Aközbek, A. Becker, V. P. Kandidov, O. G. Kosareva, and H. Schroeder, Can. J. Phys. **83**, 863 (2005).
[11] A. Couairon and A. Mysyrowicz, Phys. Rep. **441**, 47 (2007).
[12] M. Rodriguez, R. Sauerbrey, H. Wille, L. Woste, T. Fujii, Y. B. Andre, A. Mysyrowicz, L. Klingbeil, K. Rethmeier, W. Kalkner, J. Kasparian, E. Salmon, J. Yu, and J. P. Wolf, Opt. Lett. **27**, 772 (2002).
[13] A. P. Baronavski, H. D. Ladouceur, and P. G. Girardi, Experimental Observations of Electrical Arc discharges along Laser Plasma Channels, NRL/MR/6110–02-8642, 2002 (unpublished).
[14] D. F. Gordon, A. Ting, R. F. Hubbard, E. Briscoe, C. Manka, A. P. Baronavski, H. D. Ladouceur, P. W. Grounds, and P. G. Girardi, Phys. Plasmas **10**, 4530 (2003).
[15] Tz. Petrova, H. D. Ladouceur, and A. P. Baronavski, Proceedings in 58th Gaseous Electronic Conference, San Jose, 2005 (unpublished), p. 18. We have obtained a breakdown electric field of 5.7 kV cm^{-1} using a linear regression to fit the voltage measurements vs distance by Rodriguez *et al.* [12].
[16] H. D. Ladouceur, A. P. Baronavski, P. G. Girardi, and C. A. Sullivan, Electric Field Scaling and Charge Delivery via Laser-Induced Laser Plasma Channels, NRL/MR/6110–05-8914, 2005 (unpublished).
[17] M. Yamaura, Appl. Phys. Lett. **88**, 251501 (2006).
[18] P. B. Corkum, C. Rolland, and T. Rao, Phys. Rev. Lett. **57**, 2268 (1986).
[19] Teramobile online: http://www.teramobile.org
[20] M. Raizen, C. Salmon, and Q. Niu, Phys. Today **54**(8), 17 (2001).
[21] P. Rairoux, H. Schillinger, S. Niedermeier, M. Rodrigues, F. Ronneberger, R. Sauerbrey, B. Stein, D. Waite, C. Wedekind, H. Wille, L. Wöste, and C. Ziener, Appl. Phys. B: Lasers Opt. **71**, 573 (2000).

[22] N. A. Popov, Plasma Phys. Rep. **29**, 695 (2003).
[23] I. P. Shkarofsky, T. W. Johnston, and M. P. Bachynski, *The Particle Kinetics in Plasma* (Addison-Wesley, Reading, MA, 1966), Chaps. 2–5.
[24] S. Yoshida, A. V. Phelps, and L. C. Pitchford, Phys. Rev. A **27**, 2858 (1983).
[25] R. Winkler, M. Capitelli, M. Dilonardo, C. Gorse, and J. Wilhelm, Plasma Chem. Plasma Process. **6**, 437 (1986).
[26] Ts. Petrova, E. Benova, G. Petrov, and I. Zhelyazkov, Phys. Rev. E **60**, 875 (1999).
[27] This data has been developed over many years by A. V. Phelps, and coworkers at JILA: http://jilawww.colorado.edu/www/research/colldata.html
[28] J. Dutton, J. Phys. Chem. Ref. Data **4**, 577 (1975).
[29] D. K. Gupta, S. Mahajan, and P. I. John, J. Phys. D **33**, 681 (2000).
[30] J. J. Lowke, J. Phys. D **25**, 202 (1992).
[31] K. Feser and R. C. Hughes, Electra **117**, 23 (1988).
[32] S. Tzortzakis, B. Prade, M. Franco, A. Mysyrowicz, S. Huller, and P. Mora, Phys. Rev. E **64**, 057401 (2001).
[33] R. S. Sigmund, J. Appl. Phys. **56**, 1355 (1984).
[34] Y. Itikawa, J. Phys. Chem. Ref. Data **35**, 31 (2006).
[35] L. C. Pitchford and A. V. Phelps, Phys. Rev. A **25**, 540 (1982).
[36] R. D. Hake, Jr. and A. V. Phelps, Phys. Rev. **158**, 70 (1967).
[37] M. Capitelli, C. M. Ferreira, B. F. Gordiets, and A. I. Osipov, *Plasma Kinetics in Atmospheric Gases* (Springer-Verlag, Berlin, 2000), Chap. 8.
[38] H. Myers, J. Phys. B **2**, 393 (1969).
[39] D. E. Shemansky and A. L. Broadfood, J. Quant. Spectrosc. Radiat. Transf. **11**, 1401 (1971).
[40] E. Brook, M. F. A. Harrison, and A. C. H. Smith, J. Phys. B **11**, 3115 (1978).
[41] H. W. Drawin, Z. Phys. **225**, 470 (1969).
[42] E. W. McDaniel, *Collisional Phenomena in Ionized Gases* (Wiley, New York, 1964), Chap. 8.
[43] P. D. Burrow, J. Chem. Phys. **59**, 4922 (1973).
[44] M. Jinno, M. Kubo, M. Aono, and R. Itatani, Jpn. J. Appl. Phys., Part 1 **36**, 2870 (1997).
[45] V. Guerra and J. Loureiro, Plasma Sources Sci. Technol. **6**, 373 (1997); **6**, 361 (1997).
[46] P. A. Sá and J. Loureiro, J. Phys. D **30**, 2320 (1997).
[47] L. G. Piper, J. Chem. Phys. **91**, 864 (1989).
[48] L. G. Piper, J. Chem. Phys. **88**, 231 (1988); **88**, 6911 (1988).
[49] L. G. Piper, J. Chem. Phys. **87**, 1625 (1987).
[50] A. R. De Sousa, M. Touzeau, and M. Petididier, Chem. Phys. Lett. **121**, 423 (1985).
[51] W. J. Marinelli, W. J. Kessler, B. D. Green, and W. A. M. Blumberg, J. Chem. Phys. **90**, 2167 (1989).
[52] W. J. Marinelli, B. D. Green, M. A. DeFaccio, and W. A. M. Blumberg, J. Phys. Chem. **92**, 3429 (1988).
[53] M. P. Iannuzzi, J. B. Jeffries, and F. Kaufman, Chem. Phys. Lett. **87**, 570 (1982).
[54] V. V. Ivanov, K. S. Klopovsky, D. V. Lopaev, Y. A. Mankelevich, A. T. Rakhimov, and T. V. Rakhimova, IEEE Trans. Plasma Sci. **31**, 528 (2003).
[55] J. T. Gudmundsson, I. G. Kouznetsov, K. K. Patel, and M. A. Liberman, J. Phys. D **34**, 1100 (2001).
[56] B. Gordiets, C. M. Ferreira, V. Guerra, J. Loureiro, J. Nahorny, D. Pagnon, M. Touzeau, and M. Vialle, IEEE Trans. Plasma Sci. **23**, 750 (1995).
[57] V. A. Feoktistov, A. V. Mukhovatova, A. M. Popov, and T. V. Rakhimova, J. Phys. D **28**, 1346 (1995).
[58] I. A. Kossyi, A. Yu. Kostinski, A. A. Matveyev, and V. P. Silakov, Plasma Sources Sci. Technol. **1**, 207 (1992).
[59] V. Guerra and J. Loureiro, Plasma Sources Sci. Technol. **8**, 110 (1999).
[60] H. Partridge, S. R. Langhoff, C. W. Bauschlicher, and D. W. Schwenke, J. Chem. Phys. **88**, 3174 (1988).
[61] B. Gordiets, C. M. Ferreira, J. Nahorny, D. Pagnon, M. Touzeau, and M. Vialle, J. Phys. D **29**, 1021 (1996).
[62] J. A. Guthrie, R. C. Chaney, and A. J. Cunningham, J. Chem. Phys. **95**, 930 (1991).
[63] J. Zinn, C. D. Sutherland, S. N. Stone, L. M. Duncan, and R. Behnke, J. Atmos. Terr. Phys. **44**, 1143 (1982).
[64] E. W. McDaniel, V. Cermak, A. Dalgarno, E. G. Ferguson, and L. Friedman, *Ion-Molecule Reactions* (Wiley, New York, 1970).
[65] F. E. Niels, J. Chem. Phys. **52**, 408 (1970).
[66] D. Hayashi and K. Kadota, J. Appl. Phys. **83**, 697 (1998).
[67] L. M. Chanin, A. V. Phelps, and M. A. Biondi, Phys. Rev. Lett. **2**, 344 (1959).
[68] L. M. Chanin, A. V. Phelps, and M. A. Biondi, Phys. Rev. **128**, 219 (1962).
[69] B. L. Upschulte, W. J. Marinelli, and B. D. Green, J. Phys. Chem. **98**, 837 (1994).
[70] J. I. Steinfeld, S. M. Adlergolden, and J. W. Gallagher, J. Phys. Chem. Ref. Data **16**, 911 (1987).
[71] Y. Ichikawa, R. L. C. Wu, and T. Kaneda, J. Appl. Phys. **67**, 108 (1990).
[72] F. C. Fehsenfeld, A. L. Schmeltekopf, H. I. Schiff, and E. E. Ferguson, Planet. Space Sci. **15**, 373 (1967).